



Wasiuk, D. K., Khan, M. A. H., Shallcross, D. E., & Lowenberg, M. H. (2016). The impact of global aviation NO_x emissions on tropospheric composition changes from 2005 to 2011. *Atmospheric Research*, 178-179, 73-83. <https://doi.org/10.1016/j.atmosres.2016.03.012>

Peer reviewed version

Link to published version (if available):
[10.1016/j.atmosres.2016.03.012](https://doi.org/10.1016/j.atmosres.2016.03.012)

[Link to publication record in Explore Bristol Research](#)
PDF-document

University of Bristol - Explore Bristol Research

General rights

This document is made available in accordance with publisher policies. Please cite only the published version using the reference above. Full terms of use are available:
<http://www.bristol.ac.uk/red/research-policy/pure/user-guides/ebr-terms/>

The impact of global aviation NO_x emissions on tropospheric composition changes from 2005 to 2011

D.K. Wasiuk^a, M.A.H. Khan^b, D.E. Shallcross^b, M.H. Lowenberg^{a,*}

^aDepartment of Aerospace Engineering, Queen's Building, University Walk, University of Bristol, Bristol, BS8 1TR, UK

^bAtmospheric Chemistry Research Group, School of Chemistry, Cantock's Close, University of Bristol, Bristol, BS8 1TS, UK

*Author to whom correspondence should be sent

E-mail: m.lowenberg@bristol.ac.uk

Phone: +44 (0) 117 331 5555

Abstract

The impact of aviation NO_x emissions from 2005 to 2011 on the chemical composition of the atmosphere has been investigated on the basis of integrations of the 3-D global chemical and transport model, STOCHEM-CRI with the novel CRIv2-R5 chemistry scheme. A base case simulation without aircraft NO_x emissions and integrations with NO_x emissions from aircraft are inter-compared. The sensitivity of the global atmosphere to varying the quantity and the geographical distribution of the global annual aviation NO_x emissions is assessed by performing, for the first time, a series of integrations based on changing the total mass and distribution of aircraft NO_x emissions derived from air traffic movements recorded between 2005 and 2011. The emissions of NO_x from the global fleet based on actual records of air traffic movements between 2005 and 2011 increased the global tropospheric annual mean burden of O₃ by 1.0 Tg and decreased the global tropospheric annual mean burden of CH₄ by 2.5 Tg. The net NO_y and O₃ production increases by 0.5% and 1%, respectively between 2005 and 2011 in total. At cruise altitude, the absolute increase in the modelled O₃ mixing ratios is found to be up to 0.7 ppb between 2005 and 2011 at 25°N-50°N.

Keywords: Aviation NO_x, tropospheric O₃, Climate Change, STOCHEM-CRI.

1. Introduction

Nitrogen oxides, NO_x (NO + NO₂) are catalytic precursors of ozone (O₃) which can influence the oxidative capacity of the atmosphere strongly (Zhang et al., 2003; Kunhikrishnan and

Lawrence, 2004; Labrador et al., 2005). The sources of NO_x originate mainly from fossil fuel combustion and biomass burning (Denman et al., 2007), soil emission (Davidson and Kinglerlee, 1997; Ussiri et al., 2013), ammonia oxidation (Zhu et al., 2013), lightning (Chameides et al., 1977; Labrador et al., 2005), aircraft emissions (Brasseur et al., 1998; Sausen et al., 2005) and stratospheric intrusions (Lamarque et al., 1996). Aircraft NO_x is emitted predominantly at aircraft cruise altitudes from 8-12 km, which can contribute to the formation of tropospheric ozone (O₃), the third largest contributor to positive radiative forcing (Denman et al., 2007). Over the past decade, several studies showed the effects of aviation NO_x emissions on tropospheric ozone (Grewe et al., 2002; Köhler et al., 2008; Hoor et al., 2009; Hodnebrog et al., 2011; Myhre et al., 2011; Jacobson et al., 2013; Olsen et al., 2013, Gilmore et al., 2013). However, understanding the spatial and temporal distribution of aviation NO_x emissions is important for modelling aviation's climate impacts (Wilkerson et al., 2010) because the emissions are not emitted uniformly over the Earth. Moreover, the atmospheric impact of aviation NO_x emissions is heterogeneous. The temporal and spatial variability in the aviation NO_x related atmospheric impacts has been investigated by Stevenson and Derwent (2009), Gilmore et al. (2013), Köhler et al. (2013), Søvde et al. (2014), and Skowron et al. (2015).

In recent years, substantial changes in global and regional air traffic patterns have taken place and there is an evidence of strong correlation between growth rates of air traffic and aircraft emissions (e.g. an annual growth in fuel burn of 3.95% from 2004 to 2006 increased the aircraft emissions of CO₂, CO, H₂O, NO_x by ~4% per year in Wilkerson et al. (2010) study). Wasiuk et al. (2015a) presented an updated estimate of global aviation fuel burn and emissions using the database of global commercial aircraft movements in the form of a 4-D Aircraft Fuel Burn and Emissions Inventory spanning seven years (2005-2011). The 4-D Aircraft Fuel Burn and Emissions Inventory enabled a consistent global and regional trend analysis and composition of aviation's global and regional emissions. The analysis by Wasiuk (2014) showed a number of important trends: (i) a subtle but persistent change in the distribution of the total global annual NO_x emissions from aircraft emitted in the northern hemisphere was identified, (ii) between 2005 and 2011, there is a consistent decline in the annual aircraft NO_x emissions in the region of 30-60°N and conversely, a consistent rise in annual aircraft NO_x emissions in between 0°N and 30°N. (iii) the in depth analysis of the results from the 4-D Aircraft Fuel Burn and Emissions Inventory for the period of 2005-2011 revealed trends of varying growth, fluctuation and decline in the regional volumes of air

traffic (measured by the regional number of departures) concealed by the global totals. This highlighted a series of surprising relationships of the intracontinental volume of air traffic (as measured by the number of departures within region) and the emitted mass (in Tg(N)) of NO_x accounted for by the intracontinental traffic within the region between Asia, Europe, and North America. Considerable differences in the regional emission intensities of NO_x between the three regions, namely Asia, Europe, and North America which collectively accounted for 80% of the total global air traffic between 2005 and 2011 were found (Wasiuk, 2014). Therefore, it is necessary to update the understanding of the spatial and temporal distribution of global aviation NO_x emissions and their impact on tropospheric O₃, in particular.

In this study, we used a 3-D global chemistry and transport model, STOCHEM-CRI to investigate the impact of current (2005-2011) global aviation NO_x emissions on the global atmospheric composition and chemistry and the tropospheric distribution of NO_x and O₃. The sensitivity of the global atmosphere to varying the total mass and the global geographical distribution of the total global annual aircraft NO_x emissions is studied with a series of sensitivity simulations: a global 3-D spatial distribution of the annual aviation NO_x emissions derived from a detailed representation of the global fleet based on actual records of air traffic movements between 2005 and 2011 and a detailed distribution of the fuel consumption throughout the entire flight cycle is used as input into the model.

2. Model description

STOCHEM is a 3-D global Chemistry Transport Model originally developed by the UK Meteorological Office (Collins et al., 1997). The chemistry component of the model is the Common Representative Intermediates mechanism version 2 and reduction 5 (CRI v2-R5), referred to as 'STOCHEM-CRI'. The CRIv2-R5 scheme is traceable to the Master Chemical Mechanism (MCM v3.1) which includes 220 species competing in 609 reactions, with the suite of emitted non-methane VOCs represented by 22 compounds, as well as an organic aerosol representation (Utembe et al., 2010). Full details of the development of the CRIv2-R5 scheme can be found in Jenkin et al. (2008); Watson et al. (2008); Utembe et al. (2009) and Utembe et al. (2010). STOCHEM-CRI uses pre-calculated transport and physical fields to simulate chemical turnover, processes and distribution, as well as large scale dynamic processes in the troposphere by moving 50,000 constant mass air parcels around the global atmosphere. Within the air parcels, chemical species are produced and lost in reactions and photochemical dissociations, the rate coefficients for which are specified as functions of

temperature and incident light, respectively. STOCHEM-CRI's dynamical core is the same as that of Collins et al. (1997), with updates detailed in Derwent et al. (2008). The physical processes acting within each of the 50,000 air parcels are emission, dry and wet deposition, convection, and sub grid scale mixing between the air parcels (Derwent et al., 2003). The model moves air parcels by advecting their centroids with a time step of 3 h using a 4th order Runge-Kutta advection scheme. All trace gas species and aerosols are advected simultaneously, hence emission, chemistry, deposition, and removal processes are uncoupled from the advection (Collins et al., 2000). The air parcels are mapped after each advection step to a $5^\circ \times 5^\circ$ longitude and latitude resolution grid with 9 vertical levels extending up to 100 hPa (~ 16 km) (Derwent et al., 2008). The chemical evolution within the air parcel depends on the physical conditions and emissions that it encounters along its course of travel (Watson, 2007). The concentration of each chemical species is updated using backward Euler integration with a chemical time step $\Delta t = 5$ min (Collins et al., 1997). Wet deposition operates within the model on all soluble species using scavenging coefficients, and dry deposition follows a resistance approach (Derwent et al., 2008). Cloud-chemistry interactions are very complex and presently not very well understood in the STOCHEM-CRI (Collins et al., 2000). STOCHEM-CRI does not simulate stratospheric chemistry and stratospheric O_3 production is not included (Derwent et al., 2003). The model does account for the stratospheric influx of O_3 into the troposphere, as this flux is a key determinant of upper tropospheric O_3 concentrations (Stevenson et al., 2006). The O_3 influx is calculated from an ozone climatology and the local vertical winds and is added at 100 hPa (~ 16 km) (Stevenson et al., 2006). The total global stratospheric influx of O_3 is fixed at 609 Tg/yr. Any loss in species due to upwards transport into the stratosphere is neglected (Collins et al., 1997), as STOCHEM-CRI has an impenetrable upper boundary (top of the model at ~ 100 hPa and approximately at the level of the tropical tropopause) for all species other than ozone and NO_y . The aircrafts fly below upper boundary and the aircraft NO_x emissions employed in STOCHEM are all below this level. Any NO_y influx from the stratosphere is introduced as nitric acid, HNO_3 and a fixed mass ratio of O_3 to NO_y in exchange with the lower stratosphere is assumed (Stevenson et al., 2005).

STOCHEM-CRI takes three types of emissions as input: 2-D surface emissions, 3-D emissions of aircraft and lightning NO_x and a 2-D stratospheric source of NO_x and nitric acid (HNO_3). All sources of surface emissions (anthropogenic, biomass burning, vegetation, soil,

oceans, and other) are based on 2-D source maps. The global totals of all the 2-D input emissions can be found in Khan et al. (2014). Emission totals for CH₄ have been taken from the inverse model study of Mikaloff-Fletcher et al. (2004), except for the ocean emissions which are from Houweling et al. (2000). Several long time scale simulations have been performed to ensure that long lived species (e.g. CH₄) have settled down in the model and the initial fields used for CH₄ are from these long spin up runs, e.g. Johns et al. (2003). Stratospheric sources of NO_x and nitric acid (HNO₃) are calculated as 2-D inputs into the top model layer.

The distribution for lightning emission is parameterized based on the work of Price and Rind (1992) with the emissions being distributed evenly between the convective cloud top height and the surface. The lightning emissions are input on a resolution of 5° × 5° with 9 vertical levels. The emissions are scaled so that the global total NO_x emissions from lightning is 5 Tg(N)/yr. The aircraft NO_x emissions from 2005 to 2011 estimated by the 4-D Aircraft Fuel Burn and Emissions Inventory using the flight database record of the sum of all flights that took place during a particular year, on a particular route, by a particular aircraft were normalised to give global yearly NO_x emissions (Wasiuk, 2014; Wasiuk et al., 2015b) shown in Table 1. The majority of the NO_x emissions were distributed along the major intracontinental flight paths and highlighted regions of high air traffic activity; approximately half of the total global NO_x emissions from aircraft each year between 2005 and 2011 was within the North American, European, and Asian continents (Table 1). The details of the vertical distribution of the global annual aviation NO_x emissions from 2005 to 2011 can be found in the Appendix-A.

Table 1: Global and Regional emitted mass of NO_x (Wasiuk, 2014; Wasiuk et al., 2015b) for 2005-2011, all values are in Tg(N) y⁻¹.

Traffic	2005	2006	2007	2008	2009	2010	2011
Asia ↔ Asia	0.17	0.18	0.19	0.20	0.20	0.21	0.23
Europe ↔ Europe	0.09	0.10	0.11	0.11	0.10	0.11	0.12
North America ↔ North America	0.22	0.22	0.23	0.22	0.20	0.20	0.20
Other intra	0.06	0.06	0.06	0.06	0.06	0.07	0.08
Total intra	0.54	0.55	0.58	0.58	0.57	0.59	0.63
Total inter	0.50	0.52	0.55	0.57	0.56	0.59	0.63
Total (N)	1.04	1.07	1.13	1.15	1.13	1.18	1.26

Note: Other intra represents intracontinental totals for Africa ↔ Africa, Central America ↔ Central America, the Caribbean ↔ the Caribbean, Middle-East ↔ Middle-East, South America ↔ South America, Australasia ↔

Australasia). Total intra and total inter comprises of all intracontinental traffics and intercontinental traffics, respectively.

A suite of simulations were performed consisting of one base case simulation, (NoAircraft); one perturbation simulation, (Aircraft2005); and six sensitivity simulations, (Aircraft2006 – Aircraft2011). The NoAircraft simulation was based on the scenario in which the model was run with no aircraft NO_x emissions as input. The simulation, Aircraft2005 involved the NoAircraft being integrated after adding 3-D source of aircraft NO_x based on the magnitude and distribution of the emissions from 2005. In each succeeding AircraftYEAR, the 3-D aircraft NO_x source was adjusted to the magnitude and distribution of the emissions from the respective year, i.e. 2006, 2007, 2008, 2009, 2010, and 2011. In the Aircraft2006–Aircraft2011, all other emission sources and their distributions were kept fixed, and only the aircraft NO_x emissions source was varied (Table 1). All simulations were conducted with meteorology from 1998 for a period of 24 months with the first 12 allowing the model to spin up. Analysis is performed on the subsequent 12 months of data. The impact of the aviation NO_x emissions range during the time period 2005–2011 was quantified as the difference in NO_x emissions between the Aircraft2011 and Aircraft2005 scenarios.

3. Results

3.1. Global NO_y and O₃ budget

The initial addition of aircraft NO_x into the system (Aircraft2005 – NoAircraft) has the biggest impact on tropospheric composition, compared with the adjustment of the magnitude and distribution of these emissions as prescribed by the sensitivity studies for successive years as expected. Following the initial addition of aircraft NO_x into the system, the global annual mean tropospheric burdens of O₃, HNO₃, and PAN increase by 6.4 Tg (2.1%), 11.1 Gg (2.3%) and 48.2 Gg (1.3%), respectively and the global annual mean tropospheric burdens of CH₄ and CO decrease by 14.2 Tg (0.3%) and 7.5 Tg (1.9%) (see Table 2). A perturbation of NO_x can change the abundances of O₃, which would have an effect on OH and then on CH₄. The changes in CH₄ have further effects on OH and CH₄ due to the feedback effect (Fuglestad et al., 1999) resulting in a perturbation lifetime of CH₄ to approximately 12 years (IPCC, 2001). Thus 1-year spin-up time used in this study is not sufficient for surface fluxes of CH₄ to establish vertical and latitudinal gradients that reflect the atmosphere (Khodayari et al., 2015; Prather and Hsu, 2010).

The effect of aviation NO_x emissions on NO_x -induced O_3 is found to be $6.2 \text{ Tg}(\text{O}_3)/\text{Tg}(\text{N})$ in this study which is comparable with the model results of between 5.0 and $9.8 \text{ Tg}(\text{O}_3)/\text{Tg}(\text{N})$ reported in Khodayari et al. (2014), between 2.5 and $11.0 \text{ Tg}(\text{O}_3)/\text{Tg}(\text{N})$ reported in Olsen et al. (2013) and $7.9 \text{ Tg}(\text{O}_3)/\text{Tg}(\text{N})$ reported in Skowron et al. (2015). The emissions of NO_x from the global fleet based on actual records of air traffic movements between 2005 and 2011 has an impact in the troposphere with increasing the global annual burden of O_3 by 0.3% (see Table 2). As a consequence of increased O_3 levels, the global annual mean tropospheric burden of the OH radical increases by 0.4%. Consequently, the global annual mean tropospheric burdens of CH_4 and CO decrease, by 0.1 and 0.3%, respectively. The global burden of the HO_2 radical decreases by 0.1% because of the significant loss of HO_2 by reacting with NO at higher aircraft NO_x emissions. When NO_x is present in the system, HNO_3 is formed from the reaction between NO_2 and OH. A more efficient mechanism for long-range transport of NO_x around the global troposphere is via the formation of the reservoir species PAN by photochemical oxidation of carbonyl compounds in the presence of NO_x . Increased levels of NO_x between 2005 and 2011 have the effect of increasing the tropospheric burden of HNO_3 and PAN, by 0.5 and 0.2%, respectively.

Table 2: The global annual mean burden of selected trace species for the NoAircraft scenario, the difference between Aircraft2005 and NoAircraft scenarios, the difference between Aircraft2011 and Aircraft2005 scenarios as simulated by the STOCHEM-CRI

Species	Global burden NoAircraft (Gg)	(Aircraft2005 – NoAircraft)		(Aircraft2011 – Aircraft2005)	
		Absolute Change (Gg)	% Change	Absolute Change (Gg)	% Change
O_3	3.12×10^5	6.4×10^3	2.05	1.0×10^3	0.31
CH_4^*	4.41×10^6	-1.4×10^4	-0.32	-2.5×10^3	-0.06
CO	4.07×10^5	-7.5×10^3	-1.84	-1.2×10^3	-0.30
HNO_3	494.2	11.1	2.25	2.4	0.48
PAN	3805.4	48.2	1.27	7.0	0.18
PPN	52.8	-0.4	-0.76	-0.04	-0.08
OH	0.239	0.01	4.18	0.002	0.80
HO_2	26.0	-0.07	-0.27	-0.02	-0.08

*The values are not likely to be equilibrium values

The conversion of NO_x to NO_z (NO_3 , HNO_3 , N_2O_5 , PAN, PPN) dominates that of NO_z to NO_x resulting in a net $\text{NO}_x \rightarrow \text{NO}_z$ flux of 1.91×10^{35} , 1.94×10^{35} , and 1.95×10^{35} molecules on average per year for the NoAircraft, Aircraft2005, and Aircraft2011 scenarios respectively. The net $\text{NO}_x \rightarrow \text{NO}_z$ flux and the resultant NO_y ($\text{NO}_x + \text{NO}_z$) production increases by 0.4% and 0.5%, respectively between 2005 and 2011 in total. The $\text{NO}_x \rightarrow \text{NO}_z$ term is dominated by reaction $\text{NO}_2 + \text{NO}_3 \rightarrow \text{N}_2\text{O}_5$ and PAN formation which account for 55% and 34% of the

term total respectively. In contrast to HNO_3 , PAN is only sparingly soluble in water, and is not removed by deposition but thermally decomposed into its reactants, i.e. regenerating NO_x . The $\text{NO}_z \rightarrow \text{NO}_x$ term is dominated by the reverse reactions $\text{N}_2\text{O}_5 \rightarrow \text{NO}_2 + \text{NO}_3$ and PAN decomposition which account for 58% and 36% of the term total respectively.

The global annual tropospheric O_3 burden modelled in the Aircraft2011 (319 Tg) is found to be within the range of model results reported in Stevenson et al. (2006, 344 ± 39 Tg), Olsen et al. (2013, 332 ± 40 Tg) and Lee et al. (2010, 300 Tg). The production and loss terms of O_3 within this work were found to be approximately 2-fold higher than those given in Stevenson et al. (2006) and Lee et al. (2010). The production of O_3 increases by 0.2% in total between 2005 and 2011 (Table 3). The chemical production of O_3 is dominated by the reaction between HO_2 and NO (55%) because of the abundances of HO_2 over most of the globe in regions of photochemical radical production (Collins et al., 1997, Utembe et al., 2010). The second largest chemical production term (22%) is the reaction between CH_3O_2 and NO , which is due to the production of CH_3O_2 by the oxidation of CH_4 throughout the troposphere, and over polluted regions by the oxidation of longer chain hydrocarbons (Collins et al., 1997; Utembe et al., 2010). The flux through these two reaction channels increase by 0.3% and 0.2% respectively in total between 2005 and 2011. The global tropospheric O_3 loss is dominated by chemical loss as it accounts for 74% of the total loss term, while dry deposition accounts for the remaining 26%. 45% of the total global O_3 loss is due to the photolysis which experiences the smallest change (0.1% increase) between 2005 and 2011. The second largest (16.1%) chemical O_3 loss term is via reaction with HO_2 which is significant in remote regions (low NO_x condition) of the troposphere (Jacob, 1999). O_3 loss due to the HO_2 increases by 0.2% in total between 2005 and 2011. The third largest (8%) chemical O_3 loss term is via the hydroxyl radical. HO_2 produced from this reaction becomes part of either an O_3 null cycle if it reacts with NO , or one of two catalytic O_3 depletion cycles, in which case O_3 is removed from the troposphere. The flux through this reaction experiences a change (0.7% increase) between 2005 and 2011. The total loss term and net O_3 production increase by 0.2% and 1.0%, respectively, between 2005 and 2011 as seen in Table 3.

Table 3: Global tropospheric O₃ budget for the NoAircraft, Aircraft2005, and Aircraft2011 scenarios, the change from NoAircraft to Aircraft2005 and the change from Aircraft2005 to Aircraft2011 as simulated by the STOCHEM-CRI.

Species	NoAircraft (Gg)	Aircraft2005 (Gg)	% change ^a	Aircraft2011 (Gg)	% change ^b
Chemical Production					
HO ₂ + NO	4526.6	4609.0	1.8	4623.5	0.3
CH ₃ O ₂ + NO	1814.9	1836.7	1.2	1840.3	0.2
CH ₃ CO ₃ + NO	417.8	419.4	0.4	419.7	0.1
Isoprene peroxy + NO	156.9	156.7	-0.1	156.7	0.0
HOCH ₂ CH ₂ O ₂ + NO	17.0	17.0	0.2	17.0	0.0
RO ₂ + NO	444.0	444.9	0.2	445.1	0.1
Other	193.0	194.0	0.5	194.2	0.1
Stratospheric Influx	609.0	609.0	0.0	609.0	0.0
Total Production	8179.2	8286.6	1.3	8305.5	0.2
Chemical Loss					
O(¹ D) + H ₂ O → 2OH	3607.4	3635.4	0.8	3640.8	0.1
HO ₂ + O ₃ → OH + 2O ₂	1303.9	1320.5	1.3	1323.3	0.2
OH + O ₃ → HO ₂ + O ₂	652.8	678.7	4.0	683.4	0.7
Other	410.8	415.4	1.1	416.2	0.2
Dry deposition	2136.5	2164.4	1.3	2168.8	0.2
Total Loss	8111.4	8214.4	1.3	8232.5	0.2
Production - Loss	67.8	72.3	6.6	73.0	1.0

% change^a = ((Aircraft2005-NoAircraft/NoAircraft)*100) and % change^b = ((Aircraft2011-Aircraft2005/Aircraft2005)*100)

3.2. Global NO_x and O₃ distribution in the perturbation simulation

Following the initial addition of global aviation NO_x emissions into the system (Fig. 1a), NO_x mixing ratios increase predominantly in the northern hemisphere, NH (10° to 70°N) at 7.2-16.2 km with a maximum increase of more than 100% between 35°N and 45°N at 11.8-16.2 km. The global geographical distribution change in NO_x (Fig 1c) shows biggest change in between 11.8-16.2 km where it is mainly confined to the 20-60°N latitude band. The maximum increase in NO_x mixing ratios of up to 240% between 30-45°N at 11.8-16.2 km over eastern North America, and more than 130% over central mainland Europe and the northern transatlantic corridor. Following the initial addition of global aviation NO_x emissions into the system, global O₃ mixing ratios increase almost exclusively in the NH, most notably above 7.2 km, with a maximum up to 8% in 30-70°N (Fig. 2a). The differences in the concentration of NO_x across latitudes are much bigger than the differences in the

concentration of O_3 . This is due to O_3 persisting in the troposphere for longer than NO_x which also allows it to be transported around the troposphere. So while the differences in the concentration of NO_x form a landscape with sharply rising peaks, the differences in the concentrations of O_3 form a plateau. The global geographical distribution of the percent change in O_3 mixing ratios (Fig. 2c) shows a sharp increase that starts at $30^\circ N$ and goes up by 8% to $60^\circ N$ and changes into a plateau with maximum increase of up to 10% over the central mainland Europe and the northern transatlantic corridor. The absolute increase in NO_x mixing ratios at 11.8-16.2 km is found to be up to 60 ppt at $35^\circ N$ - $50^\circ N$ (Fig. 1b) which resulted in increase of O_3 mixing ratios by up to 7 ppb at $40^\circ N$ - $55^\circ N$ (Fig. 2b).

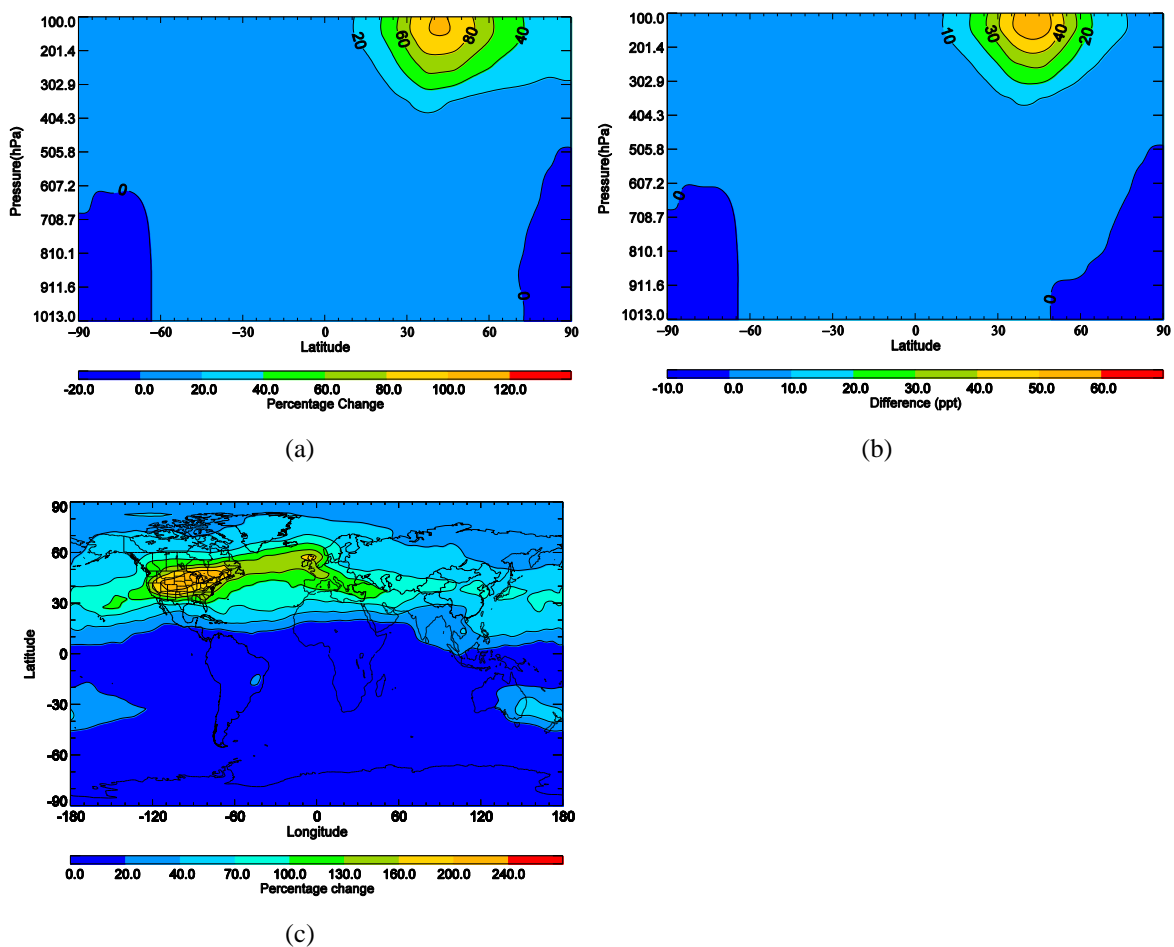


Fig. 1: Global annual (a) zonal percentage change in NO_x mixing ratios, (b) zonal absolute change in NO_x mixing ratios (c) geographical distribution of percent changes in NO_x at 11.8-16.2. Percentage change = $((Aircraft2005 - NoAircraft) / NoAircraft) * 100$ and Difference = $(Aircraft2005 - NoAircraft)$.

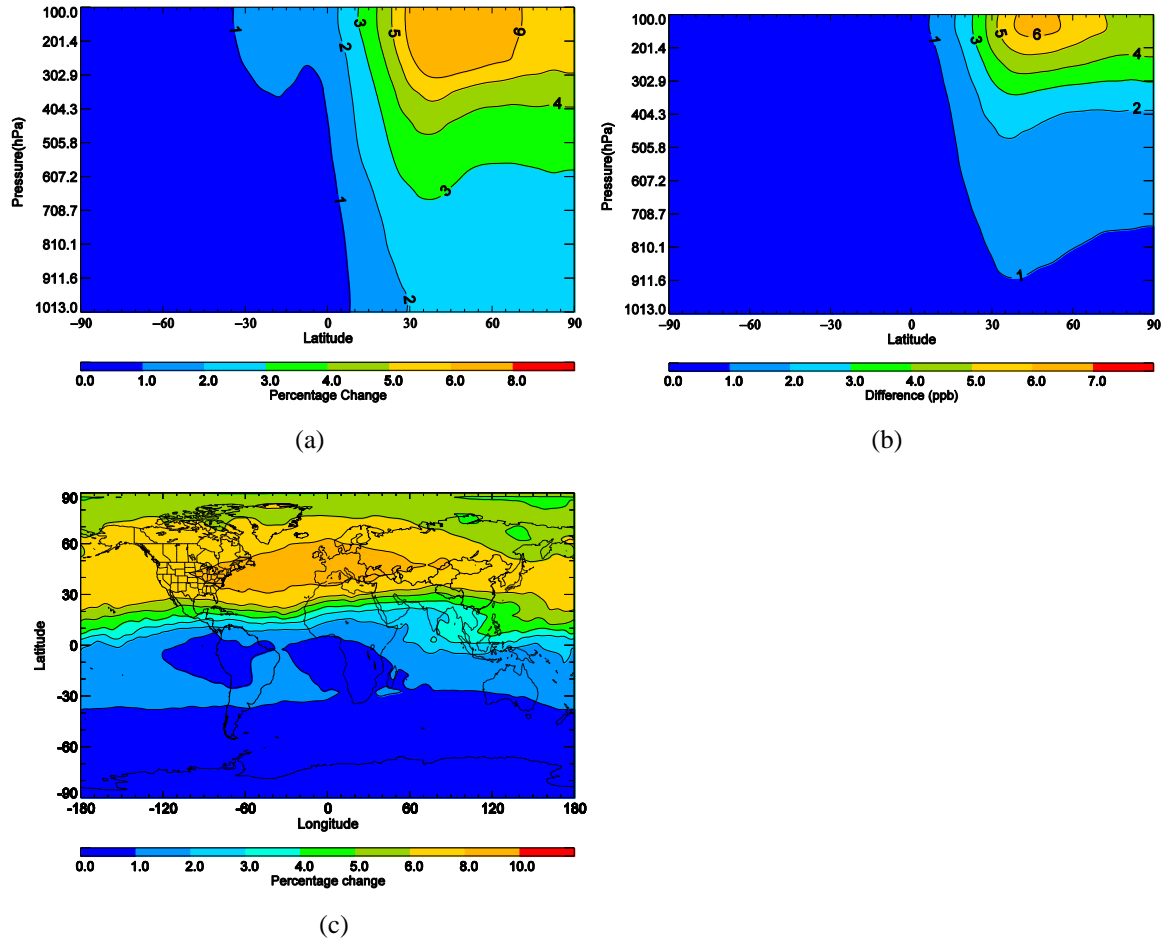
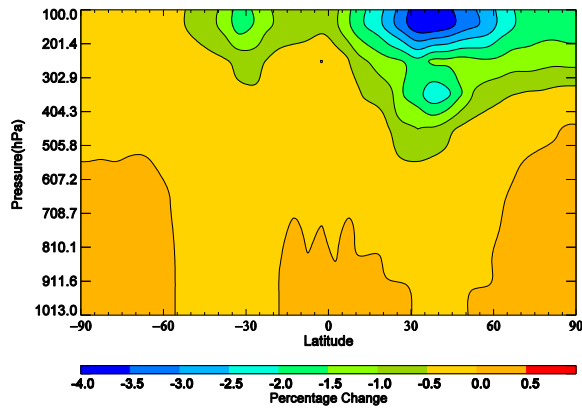


Fig. 2: Global annual (a) zonal percentage change in O₃ mixing ratios, (b) zonal absolute change in O₃ mixing ratios (c) geographical distribution of percent changes in O₃ at 11.8-16.2. Percentage change = ((Aircraft2005-NoAircraft/NoAircraft)*100) and Difference= (Aircraft2005-NoAircraft).

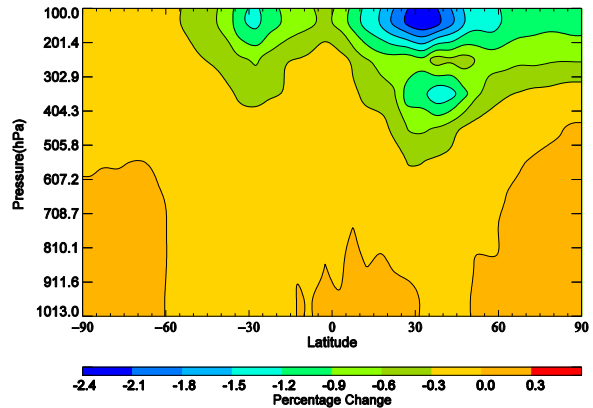
3.3. Global NO_x and O₃ distribution in the sensitivity simulations

Figure 3 shows the global inter-annual zonal distribution variation in NO_x mixing ratios with respect to the multi-annual average. Compared with the multi-annual average, the change of NO_x up to 4% (2005) and 2.4% (2006) are found in the NH between 30°N-50°N and 25°N-40°N, respectively at 11.8-16.2 km (Fig 3a and 3b). The NO_x changes up to 2% and 1.5% are also visible in the southern hemisphere (SH) between 25°S and 35°S for the simulations of the emission years, 2005 and 2006, respectively. In the simulation for emission year 2007, the NO_x change is increased up to 1.2% in the NH between 40°N-55°N at 9.2-16.2 km (Fig. 3c) and this increment is extended to the region of 40°N-80°N in the simulation for emission year 2008 (Fig. 3d). In 2009, the impact of the fall in the number of global departures on upper tropospheric NO_x mixing ratios is clearly visible as both hemispheres experience a decrease in NO_x mixing ratios (Fig. 3e). The simulation for emission year 2010 shows that the number of departures in the economies of both hemispheres began to rise as NO_x mixing ratios

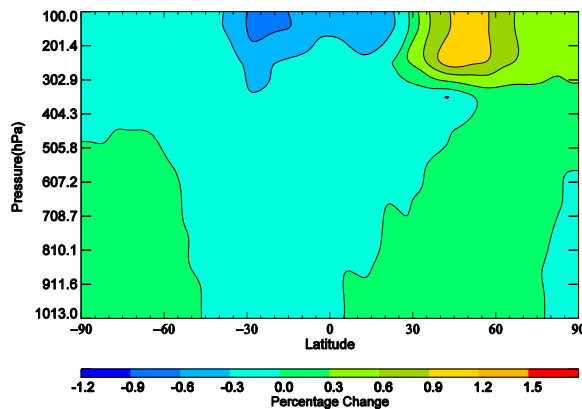
increased both hemispheres and peaked at 11.8-16.2 km in the regions of 25-35°S and 10-35°N (Fig. 3f). In the simulation for emission year 2011, the global economy improves and the region of increased NO_x extends from 40°S to 90°N, with peak between 25°N and 45°N at 11.8-16.2 km (Fig. 3g).



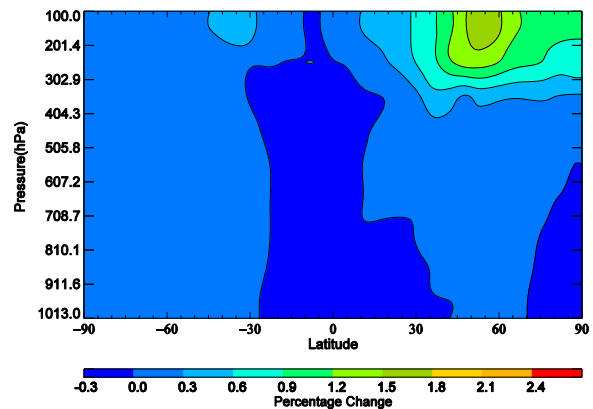
(a) ΔNO_x (in %) for 2005



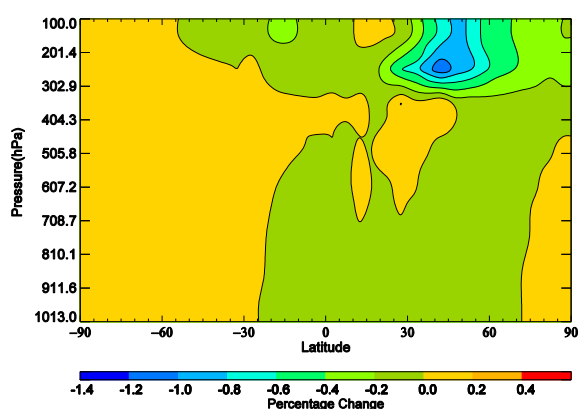
(b) ΔNO_x (in %) for 2006



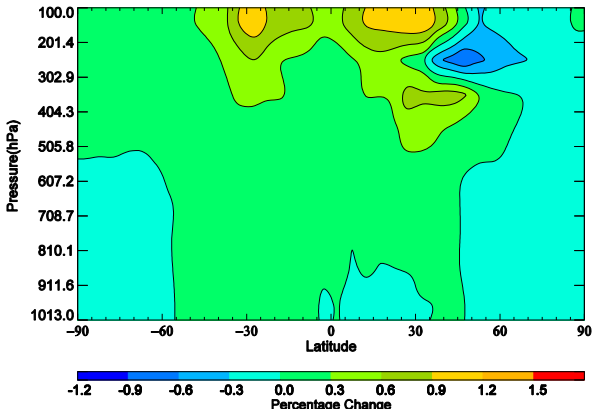
(c) ΔNO_x (in %) for 2007



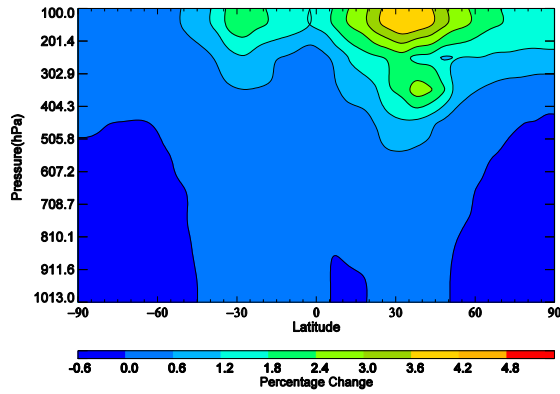
(d) ΔNO_x (in %) for 2008



(e) ΔNO_x (in %) for 2009



(f) ΔNO_x (in %) for 2010



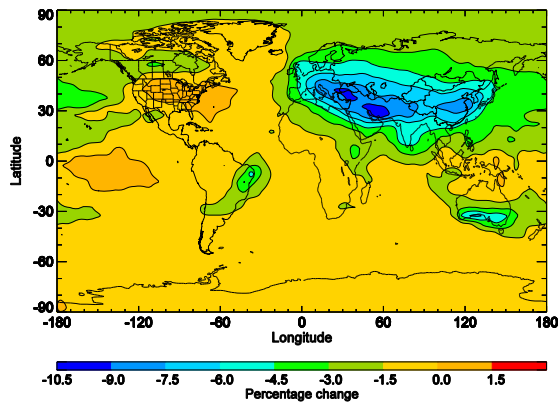
(g) ΔNO_x (in %) for 2011

Fig. 3: Global inter-annual zonal distribution variation in NO_x mixing ratios with respect to the multi-annual average. Percentage change= $((\text{AircraftYEAR}-\text{Multiannual average}) \times 100 / \text{Multiannual average})$

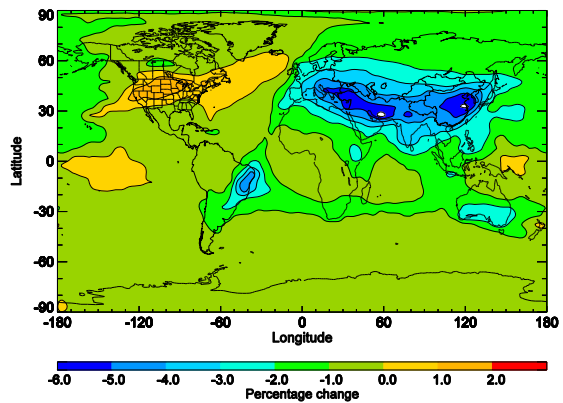
In all zonal plots of the percent change in NO_x in the seven integrations Aircraft2005 through to Aircraft2011, there are areas of negative change extending from the ground to the top of the planetary boundary layer and beyond. Overall, the difference between the changes in the upper tropospheric NO_x mixing ratios in the NH and SH due to the variation of the quantity and distribution of the global aviation NO_x emissions is found significant in the sensitivity simulations.

The global inter-annual global geographical distribution of the percent change in NO_x mixing ratios in Aircraft2005 – Aircraft2011 at 11.8-16.2 km with respect to a multi-annual average has been shown in Fig. 4. The NO_x change in the NH at 11.8-16.2 km towards more northern latitudes in the simulation for emission year 2005 (Fig. 4a) and the narrowing of the area of impact seen in the simulation for emission year 2006 is due to increased activity on the east coast of North America, central mainland Europe and the northern coast of China over Shanghai (Fig. 4b). The NO_x change in the SH is dominated over the southern coast of Australia, in southern Brazil over Rio de Janeiro, and a region extending from the north east of Africa over Ethiopia down to Madagascar in the simulations for emission year 2005 and 2006. Fig. 4c shows that the narrowing of the area of NO_x changes in the simulation for emission year 2007 is due to an increase in the NO_x mixing ratios over Europe, Australia, Asia, and north east of Africa. The appearance of heightened NO_x mixing ratios on the North America and the northern transatlantic in the simulations for emission year 2007 and 2008 is due to an increase in activity between Europe and North America (Fig. 4c and 4d). The global economic downturn of 2008 is reflected with a decreasing number of departures (2.8%) which resulted in a global decrease in NO_x emissions by 2% (Wasiuk et al., 2015b). The impact of the global economic downturn is reflected in the global troposphere experiencing

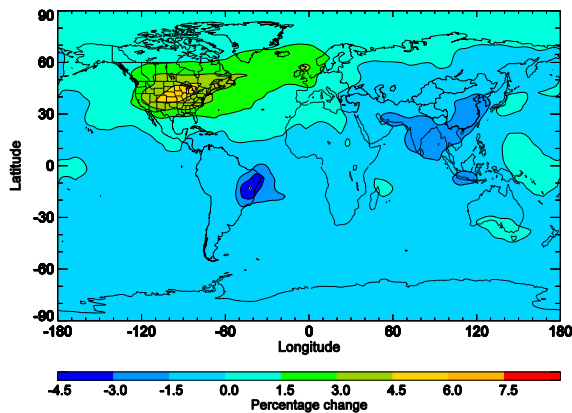
a reduction in NO_x mixing ratios in North America (Fig. 4d). If the changes in the upper tropospheric NO_x mixing ratios are linked to the levels of upper tropospheric NO_x emissions, and if the levels of upper tropospheric NO_x emissions are attributed to the volume of air traffic over a region, and in turn that to the economic circumstances of the region. In the simulation for emission year 2009, the deep decline in NO_x mixing ratios in the NH is driven primarily by a decline over North America, the northern transatlantic and in the SH by a decline over Australia, New Zealand (Fig. 4e). Fig. 4f shows the regions in the SH which continued to experience growth in the volume of air traffic in 2010, and which recovered first from the economic global downturn of 2008. It is seen that central mainland Europe, Brazil, India, China, Iran, Indonesia and Australia seem to have recovered first, that North America stabilised, and that traffic between Europe and North America suffered the most. In Fig. 4g, the economic recovery is in full swing, as evidenced by significant increases in NO_x mixing ratios in the simulation for emission year 2011. The highest increases take place over Europe, Asia and between Europe and Asia. Brazil emerges as a new NO_x mixing ratio hot spot.



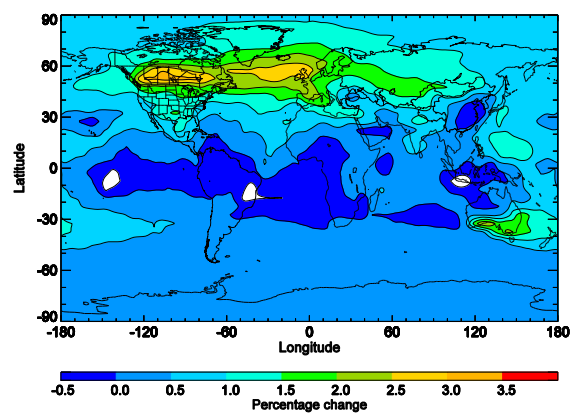
(a) ΔNO_x (in %) for 2005



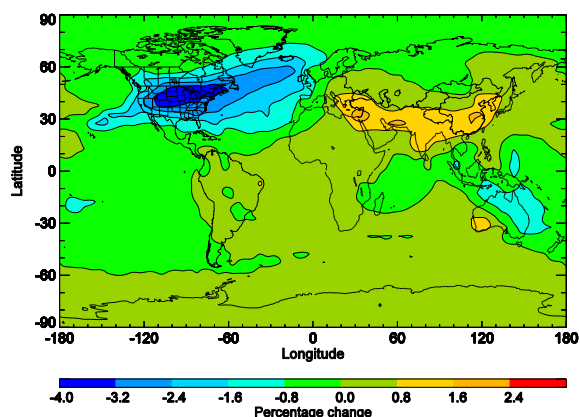
(b) ΔNO_x (in %) for 2006



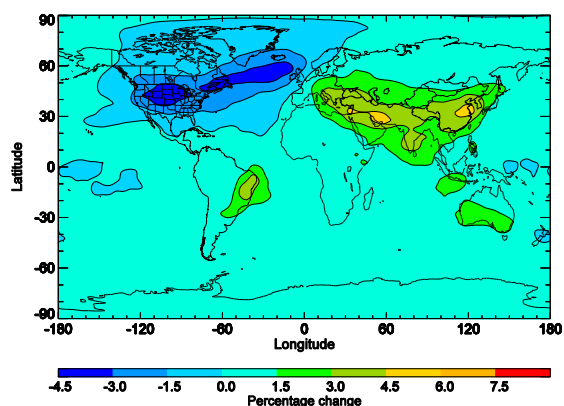
(c) ΔNO_x (in %) for 2007



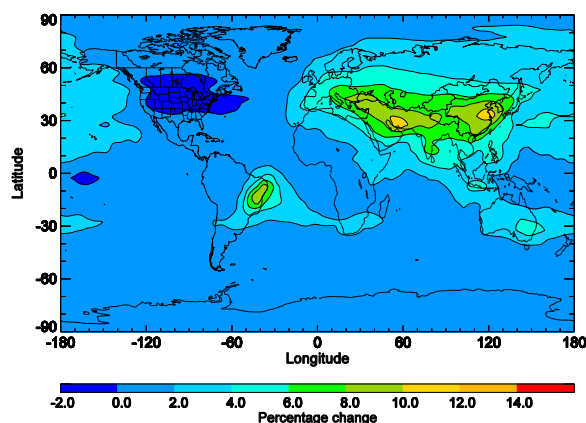
(d) ΔNO_x (in %) for 2008



(e) ΔNO_x (in %) for 2009



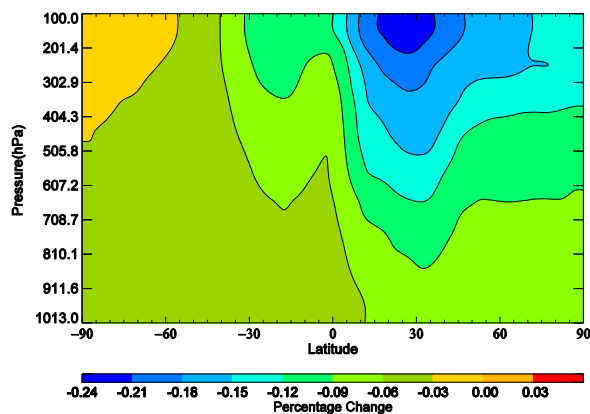
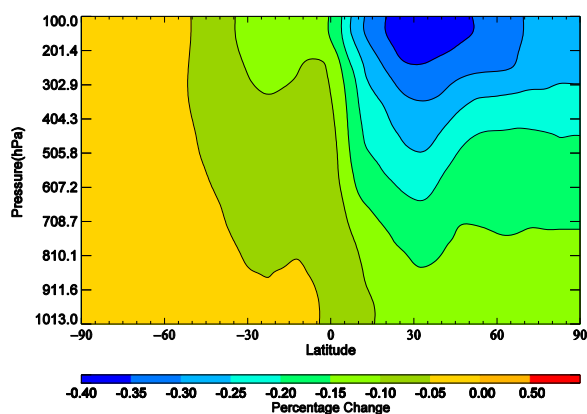
(f) ΔNO_x (in %) for 2010



(g) ΔNO_x (in %) for 2011

Fig. 4: Global inter-annual geographical distribution variation in NO_x mixing ratios with respect to the multi-annual average. Percentage change = $((\text{AircraftYEAR} - \text{Multiannual average}) * 100 / \text{Multiannual average})$

The variation in the modelled O_3 mixing ratios from year to year has been found (Fig. 5) due to the variation of the quantity and distribution of aircraft NO_x emissions from one simulation scenario to another (Fig. 3). The greatest changes in O_3 mixing ratios take place above 7.2 km in the NH, gradually propagate down to the lower levels, and are generally contained between -0.4% and 0.45%. Compared with SH, the change of O_3 mixing ratios in the NH is stronger because of the greater changes in the upper tropospheric NO_x mixing ratios in the NH.



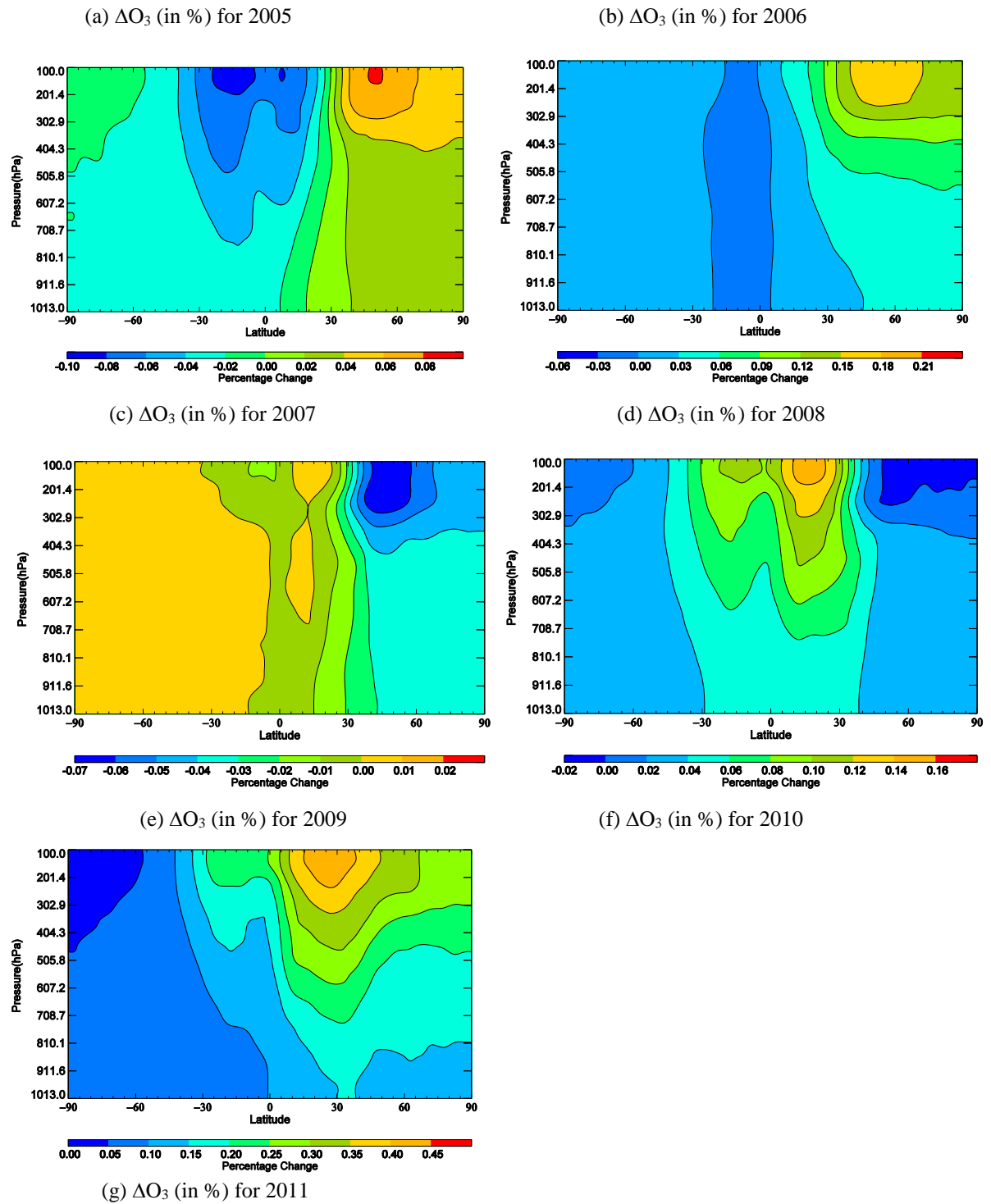
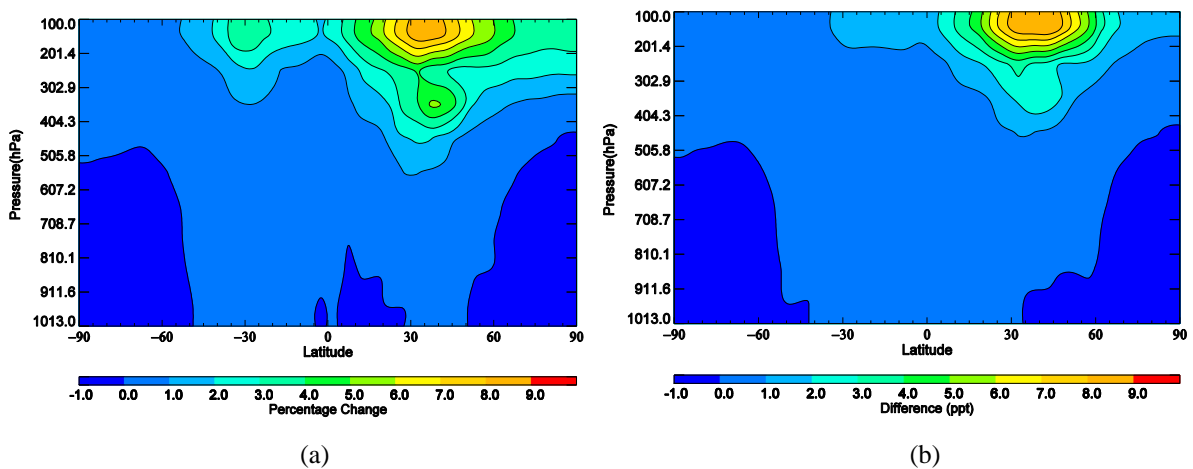
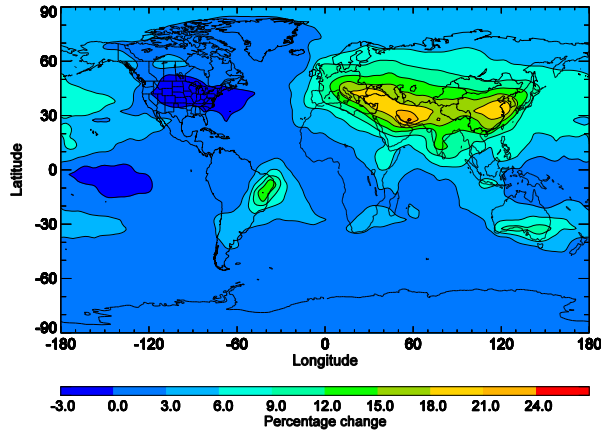


Fig 5: Global inter-annual zonal distribution variation in O_3 mixing ratios with respect to a multi-annual average. Percentage change= $((\text{AircraftYEAR}-\text{Multiannual average}) \times 100 / \text{Multiannual average})$

The global zonal and geographical distribution plots of O_3 (Fig. 7) quantify the overall change that has taken place in the distribution and magnitude of the global upper tropospheric O_3 mixing ratios above 11.8 km due to the changes in the volume and distribution of global aviation NO_x emissions between 2005 and 2011 (Fig. 6). Two areas of maximum changes of NO_x (up to 9% between 30°N and 45°N and up to 4% between 20°S and 35°S) are visible at

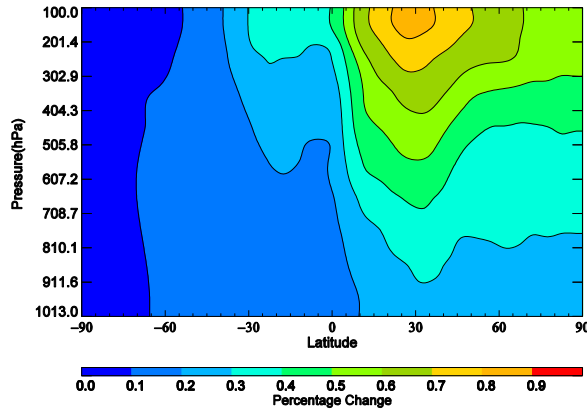
11.8-16.2 km. A small area of maximum change up to 5% has been seen at 7.2-9.2 km between 35°N and 45°N. Several areas of negative changes are also visible below the planetary boundary layer. The changes of O₃ in the NH are significant (0.8%) between 15°N and 40°N with a small change (0.4%) between 0-30°S at 9.2-16.2 km. The increase in the global concentration changes of O₃ has been found in the entire modelling domain extending from 16.2 km to ground level in the Aircraft2005-Aircraft2011 comparison (Fig. 7b). The geographical distribution plot of NO_x at 11.8-16.2 km shows that the areas of maximum NO_x change (up to 21%) are visible in the NH, over central and Eastern Europe, China, and above India, and the land masses between these regions (Fig. 6c). The maximum increases in O₃ mixing ratios downwind from the areas of maximum increases in NO_x mixing ratios. Because of the downwind transport, the shift of the higher NO_x from central Europe eastwards has resulted in higher O₃ changes (up to 1.2%) off the east coast of China, propagating further eastwards towards the western coast of North America (see Fig. 7c). Higher level of solar irradiance at lower latitudes results in faster photochemical production of O₃ (Köhler et al., 2013) which can also be responsible for increased O₃ changes in China. A peak absolute annual increase in NO_x mixing ratios of up to 9 ppt (Fig. 6b) resulted in increase in O₃ mixing ratios up to 0.7 ppb (Fig. 7b) at 25°N-50°N. A modest increase (between 0.1 and 0.2 ppb) of ground level O₃ is found between 15°N and 65°N which can affect crops and human health significantly. An increase in O₃ away from the surface will have an impact on the global radiative forcing, hence impact the greenhouse effect by enhancing it. To quantify the magnitude of this warming, the radiative forcing due to the increases in the global concentrations of O₃ modelled within this work can be calculated, but this calculation is beyond the scope of this work.



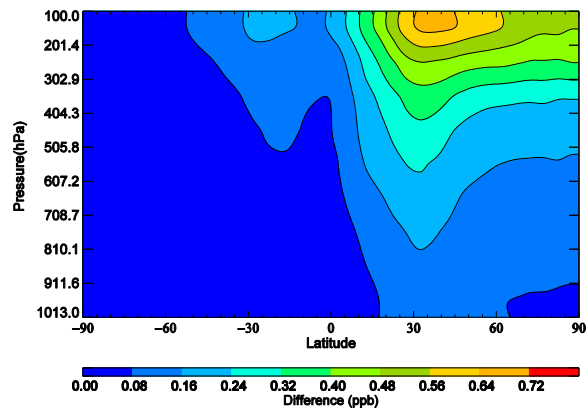


(c)

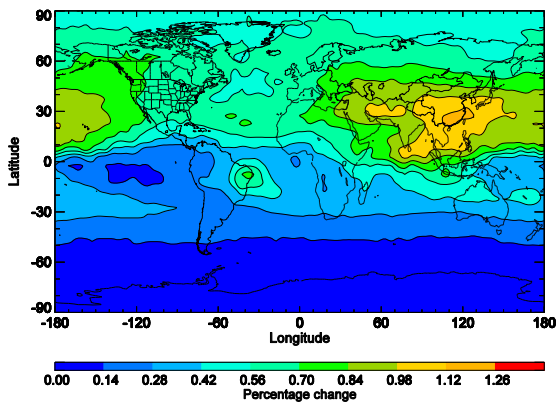
Fig. 6 Global annual zonal (a) percentage change in NO_x mixing ratios, (b) absolute change in NO_x mixing ratios (c) geographical distribution of percent changes in NO_x at 11.8-16.2. Percentage change = $((\text{Aircraft2011} - \text{Aircraft2005}) / \text{Aircraft2005}) * 100$ and Difference = $(\text{Aircraft2011} - \text{Aircraft2005})$.



(a)



(b)



(c)

Fig. 7 Global annual zonal (a) percentage change in O_3 mixing ratios, (b) absolute change in O_3 mixing ratios (c) geographical distribution of percent changes in O_3 at 11.8-16.2. Percentage change = $((\text{Aircraft2011} - \text{Aircraft2005}) / \text{Aircraft2005}) * 100$ and Difference = $(\text{Aircraft2011} - \text{Aircraft2005})$.

4. Conclusion

We used the 3-D global Lagrangian chemistry transport model, STOCHEM-CRI with the novel CRIV2-R5 chemistry scheme to investigate the spatial distribution of the aviation NO_x emissions induced changes in the concentration and distribution of global tropospheric NO_x concentrations and the radiatively active greenhouse gas, O₃ as well as their evolution for the period 2005 to 2011. The comparison of a model run with 3-D global aircraft emissions with a model run without aircraft emissions shows that the global aircraft fleet increased the global annual mean tropospheric burden of O₃ by 2.1%. The progressive manipulation of the aviation NO_x emissions between 2005 and 2011 have the effect of increasing the tropospheric burden of O₃ by 0.3%. The changes in the global annual mean burdens of the selected trace species were at most 4% that of the initial impact (perturbation simulation), hence comparably very small, while the compound impact between 2005 and 2011 was at most one fifth of the initial impact. The net NO_y and O₃ production increases by 0.5 and 1.0%, respectively between 2005 and 2011. The changes in NO_x and O₃ concentrations simulated in the sensitivity simulations are found to be one order of magnitude smaller across the longitudinal domain than those simulated in the perturbation simulation. The latitudinal variation of inter-annual changes in NO_x and O₃ concentrations is found to be significant because of the changing aviation activity. In the cruise altitude, the peak annual absolute increases in O₃ mixing ratios are found up to 7 ppb between Aircraft2005 and NoAircraft scenarios at 40°N-55°N and 0.7 ppb between Aircraft2011 and Aircraft2005 scenarios at 25°N-50°N.

Acknowledgements

We thank Dr. Michael Cooke (Met Office), Alan Knights (University of Bristol, UK), Dr. Steven Utembe (University of Melbourne, Australia), and Prof. Richard Derwent (rdscientific, Berkshire, UK) for their support with this work. We also thank the Engineering and Physical Sciences Research Council (EPSRC) (grant EP/5011214) and the Natural Environment Research Council (NERC) (grant NE/J009008/1 and NE/I014381/1), University of Bristol Faculty of Engineering and School of Chemistry for funding various aspects of this work.

References

- Brasseur, G., Cox, R., Hauglustaine, D., Isaksen, I., Lelieveld, J., Lister, D., Sausen, R., Schumann, U., Wahner, A., Wiesen, P., 1998. European scientific assessment of the atmospheric effect of aircraft emissions. *Atmos. Environ.* 32, 2329-2418.
- Chameides, W.L., Stedman, D.H., Dickerson, R.R., Rusch, D.W., Cicerone, R.J., 1977. NO_x production by lightning. *J. Atmos. Sci.* 34, 143-149.
- Collins, W.J., Stevenson, D.S., Johnson, C.E., Derwent, R.G., 1997. Tropospheric ozone in a Global-Scale Three-Dimensional Lagrangian Model and its response to NO_x emission controls. *J. Atmos. Chem.* 26(3), 223-274.
- Collins, W.J., Stevenson, D.S., Johnson, C.E., Derwent, R.G., 2000. The European regional ozone distribution and its links with the global scale for the years 1992 and 2015. *Atmos. Environ.* 34(2), 255-267.
- Davidson, E.A., Kinglerlee, W., 1997. A global inventory of nitric oxide emissions from soils. *Nutr. Cycling Agroecosyst.* 48, 37-50.
- Denman, K.L., Brasseur, G., Chidthaisong, A., Ciais, P., Cox, P.M., Dickinson, R.E., Hauglustaine, D., Heinze, C., Holland, E., Jacob, D., Lohmann, U., Ramachandran, S., da Silva Dias, P.L., Wofsy, S.C., Zhang, X., 2007. Couplings between Changes in the Climate System and Biogeochemistry. In: *Climate Change 2007: The Physical Science Basis. Contribution of Working Group I to the Fourth Assessment Report of the Intergovernmental Panel on Climate Change*. Cambridge University Press, Cambridge, United Kingdom and New York, NY, USA.
- Derwent, R.G., Stevenson, D.S., Doherty, R.M., Collins, W.J., Sanderson, M.G., 2008. How is surface ozone in Europe linked to Asian and North American NO_x emissions? *Atmos. Environ.* 42, 7412-7422.
- Derwent, R.G., Collins, W.J., Jenkin, M.E., Johnson, C.E., Stevenson, D.S., 2003. The global distribution of secondary particulate matter in a 3-D Lagrangian chemistry transport model. *J. Atmos. Chem.* 44(1), 57-95.
- Fuglestad, J.S., Berntsen, T.K., Isaksen, I.S.A., Mao, H., Liang, X.-Z., Wang, W.-C., 1999. Climatic forcing of nitrogen oxides through changes in tropospheric ozone and methane; global 3D model studies. *Atmos. Environ.* 33, 961-977.
- Gilmore, C.K., Barrett, S.R.H., Koo, J., Wang, Q., 2013. Temporal and spatial variability in the aviation NO_x-related O₃ impact. *Environ. Res. Lett.* 8(3), 034027 (8pp).
- Grewe, V., Dameris, M., Fichter, C., Sausen, R., 2002. Impact of aircraft NO_x emissions. Part I: Interactively coupled climate-chemistry simulations and sensitivities to climate-chemistry feedback, lightning and model resolution. *Meteorol. Z.* 11, 177-186.
- Hodnebrog, Ø., Berntsen, T.K., Dessens, O., Gauss, M., Grewe, V., Isaksen, I.S.A., Koffi, B., Myhre, G., Olivie, D., Prather, M.J., Pyle, J.A., Stordal, F., Szopa, S., Tang, Q., van Velthoven, P., Williams, J.E., Ødemark, K., 2011. Future impact of non-land based traffic emissions on atmospheric ozone and OH-an optimistic scenario and a possible mitigation strategy. *Atmos. Chem. Phys.* 11, 11293-11317.

- Hoor, P., Borken-Kleefeld, J., Caro, D., Dessens, O., Endresen, O., Gauss, M., Grewe, V., Hauglustaine, D., Isaksen, I.S.A., Jöckel, P., Lelieveld, J., Myhre, G., Meijer, E., Olivier, D., Prather, M., Poberaj, C.S., Shine, K.P., Stachelin, J., Tang, Q., van Velthoven, P., Sausen, R., 2009. The impact of traffic emissions on atmospheric ozone and OH: results from QUANTIFY. *Atmos. Chem. Phys.* 9, 3113-3136.
- Houweling, S., Dentener, F., Lelieveld, J., Walter, B., Dlugokencky, E., 2000. The modelling of tropospheric methane- How well can point measurements be produced by a global model? *J. Geophys. Res.* 105, 8981-9002.
- Intergovernmental Panel on Climate Change (IPCC), Climate change 2001: the scientific basis. In: Houghton, J.T., Ding, Y., Griggs, D.J., Noguer, M., van der Linden, P.J., Dai, X., Maskell, K., Johnson, C.A. (Eds.), Contribution of Working Group I to the Third Assessment Report of the Intergovernmental Panel on Climate Change. Cambridge University Press, Cambridge, United Kingdom and New York, NY, USA. Pp. 996.
- Jacob, D.J., 1999. Introduction to atmospheric chemistry. Princeton University Press, Princeton, USA.
- Jacobson, M.Z., Wilkerson, J.T., Naiman, A.D., Lele, S.K., 2013. The effects of aircraft on climate and pollution. Part II: 20-year impacts of exhaust from all commercial aircraft worldwide treated individually at the subgrid scale. *Faraday Discuss.* 165, 369-382.
- Jenkin, M.E., Watson, L.A., Utembe, S.R., Shallcross, D.E. 2008. A Common Representative Intermediate (CRI) mechanism for VOC degradation. Part-1: gas phase mechanism development. *Atmos. Environ.* 42, 7185-7195.
- Johns, T.C., Gregory, J.M., Ingram, W.J., Johnson, C.E., Jones, A., Lowe, J.A., Mitchell, J.F.B., Roberts, D.L., Sexton, D.M.H., Stevenson, D.S., Tett, S.F.B., Woodage, M.J., 2003. Anthropogenic climate change for 1860 to 2100 simulated with the HadCM3 model under updated emissions scenarios. *Climate Dynamics* 20, 583-612.
- Khan, M.A.H., Cooke, M.C., Utembe, S.R., Xiao, P., Derwent, R.G., Jenkin, M.E., Archibald, A.T., Maxwell, P., Morris, W.C., South, N., Percival, C.J., Shallcross, D.E., 2014. Reassessing the photochemical production of methanol from peroxy radical self and cross reactions using the STOCHEM-CRI global chemistry and transport model. *Atmos. Environ.* 99, 77-84.
- Khodayari, A., Olsen, S.C., Wuebbles, D.J., Phoenix, D.B., 2015. Aviation NO_x-induced CH₄ effect: Fixed mixing ratio boundary conditions versus flux boundary conditions. *Atmos. Environ.* 113, 135-139.
- Köhler, M.O., Rädcl, G., Dessens, O., Shine, K.P., Rogers, H.L., Wild, O., Pyle, J.A., 2008. Impact of perturbations to nitrogen oxide emissions from global aviation. *J. Geophys. Res.* 113, D11305.
- Köhler, M.O., Rädcl, G., Shine, K.P., Rogers, H.L. and Pyle, J.A., 2013. Latitudinal variation of the effect of aviation NO_x emissions on atmospheric ozone and methane and related climate metrics. *Atmos. Environ.* 64, 1-9.

573 Kunhikrishnan, T., Lawrence, M.G., 2004. Sensitivity of NO_x over the Indian Ocean to
574 emissions from the surrounding continents and nonlinearities in atmospheric chemistry
575 responses. *Geophys. Res. Lett.* 31, L15109.

576 Labrador, L.J., von Kuhlmann, R., Lawrence, M.G., 2005. The effects of lightning produced
577 NO_x and its vertical distribution on atmospheric chemistry: sensitivity simulations with
578 MATCH-MPIC. *Atmos. Chem. Phys.* 5, 1815-1834.

579 Lamarque, J.F., Brasseur, G.P., Hess, P.G., Muller, J.F., 1996. Three-dimensional study of
580 the reactive contributions of the different nitrogen sources in the troposphere. *J. Geophys.*
581 *Res.* 101, 22955-22968.

582 Lee, D.S., Pitari, G., Grewe, V., Gierens, K., Penner, J.E., Petzold, A., Prather, M.J.,
583 Schumann, U., Bais, A., Bernsten, T., Iachetti, D., Lim, L.L., Sausen, R., 2010. Transport
584 impacts on atmosphere and climate: Aviation. *Atmos. Environ.* 44(37), 4678-4734.

585 Mikaloff-Fletcher, E., Tans, P.P., Bruhwiler, L.M., Miller, J.B., Heimann, M., 2004. CH₄
586 sources estimated from atmospheric observations of CH₄ and its ¹³C/¹²C isotopic ratios: 1.
587 Inverse modelling of source processes. *Global Biogeochem. Cycles.* 18, GB4004.

588 Myhre, G., Shine, K.P., Rädel, G., Gauss, M., Isaksen, I.S.A., Tang, Q., Prather, M.J.,
589 Williams, J.E., van Velthoven, P., Dessens, O., Koffi, B., Szopa, S., Hoor, P., Grewe, V.,
590 Borken-Kleefeld, J., Bernsten, T.K., Fuglestad, J.S., 2011. Radiative forcing due to changes
591 in ozone and methane caused by the transport sector. *Atmos. Environ.* 45, 387-394.

592 Olsen, S.C., Brasseur, G.P., Wuebbles, D.J., Barrett, S.R.H., Dang, H., Eastham, S.D.,
593 Jacobson, M.Z., Khodayari, A., Selkirk, H., Sokolov, A., Unger, N., 2013. Comparison of
594 model estimates of the effects of aviation emissions on atmospheric ozone and methane.

595 Prather, M.M.J. and Hsu, J., 2010. Coupling of nitrous oxide and methane by global
596 atmospheric chemistry. *Science* 330, 952-954.

597 Price, C., and Rind, D., 1992. A simple lightning parameterization for calculating global
598 lightning distributions. *J. Geophys. Res. Atmos.* 97, 9919-9933.

599 Sausen, R., Isaksen, I., Grewe, V., Hauglustaine, D., Lee, D.S., Myhre, G., Köhler, M.O.,
600 Pitari, G., Schumann, U., Stordal, F., Zerefos, C., 2005. Aviation radiative forcing in 2000:
601 an update of IPCC(1999). *Meteorol. Zeit* 114, 555-561.

602 Seinfeld, J.H., Pandis, S.N., (Eds.), 2006. *Atmospheric chemistry and physics: from air*
603 *pollution to climate change*, John Wiley & Sons Ltd., New Jersey, USA.

604 Skowron, A., Lee, D.S., De León, R.R., 2015. Variation of radiative forcings and global
605 warming potentials from regional aviation NO_x emissions. *Atmos. Environ.* 104, 69-78.

606 Søvde, O.A., Matthes, S., Skowron, A., Iachetti, D., Lim, L., Owen, B., Hodnebrog, Ø., Di
607 Genova, G., Pitari, G., Lee, D.S., Myhre, G., and Isaksen, I.S.A., 2014. Aircraft emission
608 mitigation by changing route altitude: A multi-model estimate of aircraft NO_x emission
609 impact on O₃ photochemistry. *Atmos. Environ.* 95, 468-79.

610 Stevenson, D.R., Doherty, R., Sanderson, M., Johnson, C., Collins, B., Derwent, D., 2005.
611 Impacts of climate change and variability on tropospheric ozone and its precursors. *Faraday*
612 *Discuss.* 130, 1-17.

613 Stevenson, D.S., Dentener, F.J., Schultz, M.G., Ellingsen, K., Van Noije, T.P.C., Wild, O.,
614 Zeng, G., Amann, M., Atherton, C.S., Bell, N., Bergmann, D.J., Bey, I., Butler, T., Cofala, J.,

- Collins, W.J., Derwent, R.G., Doherty, R.M., Drevet, J., Eskes, H.J., Fiore, A.M., Gauss, M., Hauglustaine, D.A., Horowitz, L.W., Isaksen, I.S.A., Krol, M.C., Lamarque, J.-F., Lawrence, M.G., Montanaro, V., Müller, J.-F., Pitari, G., Prather, M.J., Pyle, J.A., Rast, S., Rodriguez, J.M., Sanderson, M.G., Savage, N.H., Shindell, D.T., Strahan, S.E., Sudo, K., Szopa, S., 2006. Multimodel ensemble simulations of present-day and near-future tropospheric ozone. *J. Geophys. Res.* 111, D08301.
- Stevenson, D.S., Derwent, R.G., 2009. Does the location of aircraft nitrogen oxide emissions affect their climate impact? *Geophys. Res. Lett.* 36, L17810.
- Ussiri, D.A.N., Lal, R., *Soil emission of nitrous oxide and its mitigation*. Dordrecht: Springer, 2013.
- Utembe, S.R., Watson, L.A., Shallcross, D.E., Jenkin, M.E., 2009. A Common Representative Intermediates (CRI) mechanism for VOC degradation. Part 3: Development of a secondary organic aerosol module. *Atmos. Environ.* 43, 1982-1990.
- Utembe, S.R., Cooke, M.C., Archibald, A.T., Jenkin, M.E., Derwent, R.G., Shallcross, D.E., 2010. Using a reduced Common Representative Intermediates (CRI v2-R5) mechanism to simulate tropospheric ozone in a 3-D Lagrangian chemistry transport model. *Atmos. Environ.* 44, 1609-1622.
- Wasiuk, D.K., 2014. Modelling aircraft emissions and their impact on atmospheric composition and ozone. PhD Thesis. University of Bristol, UK.
- Wasiuk, D.K., Lowenberg, M.H., Shallcross, D.E., 2015a. An aircraft performance model implementation for the estimation of global and regional commercial aviation fuel burn and emissions. *Transport. Res. Part D* 35, 142-159.
- Wasiuk, D.K., M.A.H. Khan, Shallcross, D.E., Lowenberg, M.H., 2015b. An aircraft fuel burn and emissions inventory for 2005-2011. *Atmos. Environ.* (Submitted).
- Watson, L.A., Shallcross, D.E., Utembe, S.R., Jenkin, M.E., 2008. A Common Representative Intermediate (CRI) mechanism for VOC degradation. Part 2: gas phase mechanism reduction. *Atmos. Environ.* 42(31), 7196-7204.
- Watson, L.A., 2007. Development and application of chemical mechanisms in atmospheric modelling. PhD Thesis. University of Bristol, UK.
- Wilkerson, J.T., Jacobson, M.Z., Malwitz, A., Balasubramanian, S., Wayson, R., Fleming, G., Naiman, A.D., Lele, S.K., 2010. Analysis of emission data from global commercial aviation: 2004 and 2006. *Atmos. Chem. Phys.* 10(13), 6391-6408.
- Zhang, R., Tie, X., Bond, D.W., 2003. Impacts of anthropogenic and natural NO_x sources over the U.S., on tropospheric chemistry. *PNAS* 100(4), 1505-1509.
- Zhu, X., Burger, M., Doane, T.A., Horwath, W.R., 2013. Ammonia oxidation pathways and nitrifier denitrification are significant sources of N₂O and NO under low oxygen availability. *PNAS* 110(6), 6328-6333.